Armenian Journal of Physics, 2022, vol. 15, issue 4, pp. 125-130

Application of EPR Spectroscopy for Investigation of Antisite Defects in Yttrium-Aluminum Garnet

H.R. Asatryan

Ioffe Institute, St. Petersburg, 194021 Russia

E-mail: hike.asatryan@mail.ioffe.ru

(Received: August 29, 2022; Revised: September 30, 2022; Accepted: October 7, 2022)

Abstract. Paramagnetic Ce^{3+}, Tb^{3+} and Ho^{3+} centers in the yttrium position in yttrium aluminum garnet (YAG) crystals investigated by the EPR spectroscopy. Along with the main EPR signals of Ce^{3+} and non-Kramers Tb^{3+} ions located in a regular environment a number of new centers with less lines intensity with different g-factors and zero-field splitting observed. The number of lines and the symmetry of these centers indicate that they belong to cerium and terbium ions, near which there are Y_{Al} antisite defects (Y^{3+} in octahedral positions of Al^{3+}) or Al_Y (Al^{3+} in dodecahedral positions of Y^{3+}). In addition to the main EPR signals of non-Kramers Ho^{3+} ions located in Y^{3+}, a number of less intense lines with different parameters also attributed to antisite defects.

Keywords: electron paramagnetic resonance, yttrium-aluminum garnet, rare earth elements, antisite defects

DOI: 10.54503/18291171-2022.15.4-125

1. Introduction

Garnet crystals activated by rare-earth ions are widely used in quantum electronics and optoelectronics, employed as scintillators in nuclear physics and medical diagnostics; they are also promising systems for quantum calculations [1–5].

Growth of these crystals from the melt can accompanied by appearance of transposition defects, also called antisite defects. In yttrium-aluminum garnet (YAG) $Y_3Al_5O_{12}$ crystals they appear, when Al^{3+} ions are replaced by Y^{3+} ions (denoted as Y_{Al}) or when dodecahedral Y^{3+} is replaced by Al^{3+} (Al_Y). Theoretical calculations of the formation energy of various defects in YAG crystals have shown that the antisite defects dominate among intrinsic defects, since their formation energy is lower than that of Frenkel and Schottky defects [6–8]. Calculated energies of crystal lattice distortions caused by the antisite atom $Y_{Al}(a)$ agree well with the results obtained by the EXAFS measurements. First-principle simulations of the atomic and electronic structure of the antisite defects in YAG based on the density functional theory performed in [9, 10]. According to these studies, substitution of yttrium for octahedral positions of aluminum $Y_{Al}(a)$ is the most favorable among all possible ways of insertion of additional yttrium cations in the YAG structure, and the calculated concentrations of defects of this kind agree well with experimental estimates [8]. Al_Y substitution has higher formation energy even at the excessive content of Al_2O_3, which points to a small probability for formation of defects of this type. Antisite defects result in appearing of electron traps and influence remarkably the recombination processes and luminescence decay time in garnet-based scintillators [11, 12]. Therefore, investigations of antisite defects are important from the practical point of view, to improve scintillators based on cerium-containing garnets for example. Obviously, progress in these fields depends in many respects on the degree of understanding of the spectroscopic properties of the considered crystals and development on this basis of methods for producing crystals with desired parameters. One of the direct methods of investigation of the spectroscopic properties of materials is electron paramagnetic resonance (EPR) which makes it possible to determine the chemical and charge states of an impurity center, its local symmetry, the

composition of the nearest environment, the structure of energy levels, the specific features of the interaction with the crystal lattice, etc.

Antisite defects are not paramagnetic, so their direct observation by means of EPR is impossible. However, due to significant difference in the ionic radii (R_{Al}^{3+}= 0.57 Å, R_Y^{3+} = 1.02 Å) replacement of Al^{3+} ions by Y^{3+} and vice versa should lead to a significant distortion of the crystal lattice near the paramagnetic center. Oxygen ions, belonging at the same time to the environment of the paramagnetic center and of the antisite defect, shifted. Distortions in the nearest surrounding can thus make the effect of the antisite defects observable in the EPR spectra of the paramagnetic centers situated near the defect positions. Ce^{3+} ions were studied in YAG by EPR and lines of lower intensity were observed in [13] along with intensive main EPR lines of Ce^{3+}. They ascribed to the Ce^{3+} ions having an antisite defect Y_{Al} and Al_Y in their environment. EPR spectra of Tb^{3+} and satellite lines in YAG at 94 and 130 GHz obtained recently and reported in [14]. Ho^{3+} ions were studied in YAG by wide-band EPR and a number of lines of lower intensity were observed [17].

2. Experimental date and discussion

$Y_3Al_5O_{12}$:Ce, $Y_3Al_5O_{12}$:Tb and $Y_3Al_5O_{12}$:Ho^{3+} single crystals were grown in the Institute for Physical Research of the National Academy of Sciences of Armenia (Ashtarak) in molybdenum containers using oriented crystallization by the vertical Bridgman method [15, 16].

Ce^{3+} ions have one unpaired 4*f* electron. Its ground state is split due to the spin-orbital interaction and crystalline field. The ground state with the electron configuration $4f^1$ has two levels $^2F_{5/2}$ and $^2F_{7/2}$ with the gap of about 2000 cm^{-1} between them. The second and third Kramers doublets in Ce^{3+} possess high energies in YAG (228 and 587 cm^{-1}), and hence, EPR transitions are observed only between the components of the lower Kramers doublet. EPR spectra of Ce^{3+} can be described by the spin Hamiltonian orthorhombic symmetry using the effective spin of S = 1/2 and an anisotropic g factor [14].

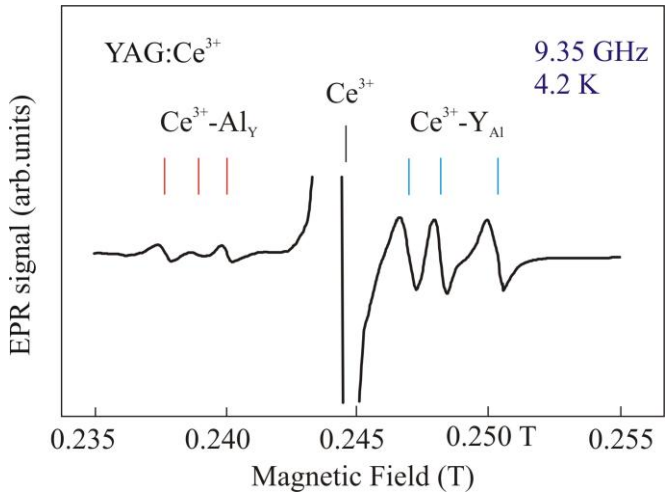

Fig. 1. EPR spectrum of the main and satellite lines of the Ce^{3+} ions in YAG single crystal for the orientation **B** || [001] at frequency ν = 9.35 GHz and T = 4.2 K.

Fig. 1 shows a fragment of the Ce^{3+} EPR spectrum recorded at X-band (9.35 GHz) in the YAG: Ce crystal in the **B** || [001] orientation. Apart from the central intensive line the three most intensive additional lines marked in blue in spectrum corresponds to the peaks in the spectra assigned to the Ce^{3+} ions having an antisite defect of the Y_{Al} type in their environment. The g factors for these lines in higher fields (g_z = 2.7, 2.70 and 2.67) are smaller than for the cerium ions in the regular environment: g_z = 2.74. Parameters of the **g** tensor depend on the crystalline field in the disposition point of Ce^{3+} and are thus sensitive to changes in the nearest environment. Three less

intense lines marked in red in fig. 1 on the lower-field side with g_z = 2.81, and 2.97 are assigned to cerium ions associated with an antisite defect of the Al_Y type.

EPR spectra of Tb^{3+} in YAG at 94 and 130 GHz obtained recently and reported in Ref. [14]. The zero-field splitting Δ between the lowest singlet levels of the non-Kramers quasi-doublet of the Tb^{3+} ($4f^8$, the ground state $^7F_6$) is very sensitive to the symmetry of the environment and, hence, to the presence of defects near the paramagnetic ions. As in the case of Ce^{3+} ions, weaker EPR peaks also observed and assigned to the terbium paramagnetic centers with altered parameters. Terbium has one stable isotope ^{159}Tb (natural abundance 100%) with the nuclear spin of I = 3/2, and hence the EPR spectrum contains four equidistant lines of the hyperfine structure.

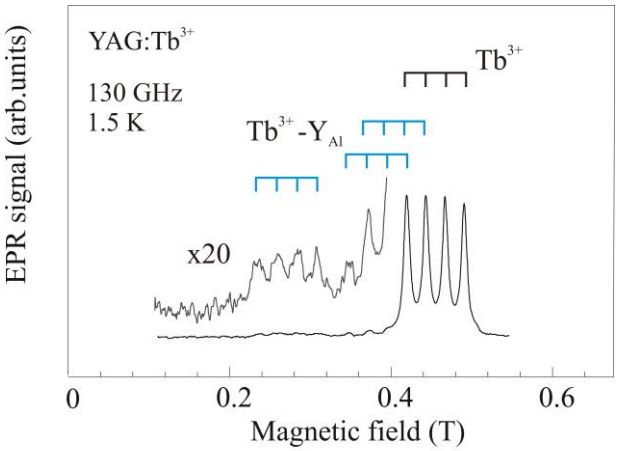

Fig. 2. EPR spectrum $Y_3Al_5O_{12}$:Tb at a frequency of 130 GHz with orientation of external magnetic field **B** || [001]. EPR lines of the main Tb^{3+} (black) and additional centers Tb^{3+} (blue).

The centers of Tb^{3+} in YAG with regular environment give the most intense EPR lines presented in Fig. 2 (the hyperfine quartet marked in black) with zero-field splitting Δ = 81.1 GHz. The spectrum, in addition to these main centers, contains three weaker EPR lines for other types of terbium centers, labelled in Fig. 2 (blue lines). They show the same hyperfine structure as the main centers, and their energy levels differ from Tb^{3+} by the value of zero-field splitting. The zero-field splitting Δ of these three additional Tb^{3+} centers in YAG (Fig. 2) are larger (93.5, 98.03 and 115.1 GHz) than for the main center type. An increase in the splitting Δ for Tb^{3+} means that the O^{2-} ions shift closer to the paramagnetic center (compression of the oxygen dodecahedron). It can be concluded that the observed satellite peaks belong to Tb^{3+} ions associated with the $Y_{Al(a)}$ type antisite defects. Angular dependences for these centers are similar to the dependence for the main center of Tb^{3+}, so these centers may identified as Tb^{3+} ions in dodecahedral positions of the garnet lattice.

Cerium has no stable odd isotopes, so its EPR spectra do not show hyperfine structure which could relate unambiguously to cerium ions. The conclusion that the weak signals belonged to Ce^{3+} made in [13] based on the similarity of the orientation and temperature dependences. In the case of Tb^{3+} ions with the nuclear spin of I = 3/2, the weak satellite EPR signals show a clear hyperfine structure with the same splitting and can be interpreted unambiguously as in the main Tb^{3+} ions occupying Y^{3+} positions in the regular environment.

Recently, additional centers of Tb^{3+} ions with a splitting Δ smaller (68.3 and 76.4 GHz) than that of the regular center have also discovered. Such centers seem to belong to a decompressed oxygen dodecahedron, which corresponds to the substitution of the nearest yttrium node with Tb^{3+}, with a smaller ionic radius of Al^{3+} (an antisite defect of the Al_Y type). Figure 3 shows a fragment of the high frequency EPR spectrum with indication of the corresponding new additional centers with smaller Δ (red lines). EPR lines of the main Tb^{3+} in fig. 3 are marked in black, the lines of the Tb^{3+} centers with larger Δ (Tb^{3+} with Y_{Al} antisite defect) are marked blue. More detailed studies of the

Tb^{3+} centers with smaller Δ are needed to elucidate the number of these centers and their angular dependences.

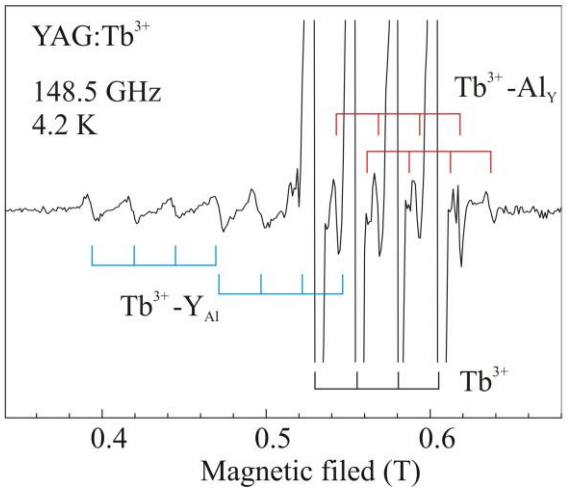

Fig. 3. EPR spectrum of $Y_3Al_5O_{12}$:Tb at a frequency of 148.5 GHz with orientation of external magnetic field **B** || [001].

Different values of the parameter g and Δ give an evidence of different distortions of the crystalline field. Evidently, substitutions $Y^{3+} \rightarrow Al^{3+}$ or $Al^{3+} \rightarrow Y^{3+}$ that occur near the impurity rare earth Tb^{3+} or Ce^{3+} ions will lead to quite different distortions of oxygen polyhedra: stretching or compression, respectively.

To explain the amount of the additional paramagnetic centers of terbium and cerium, consider the structure of the environment of a dodecahedral center in the YAG crystalline lattice, where these ions are localized, and possible positions of the nearest antisite defects Y_{Al} occupying octahedral Al positions *a*. There are 10 octahedral Al^{3+} ions sharing common oxygen ions in the environment of the Y^{3+} position. Three possible distances from the impurity ion of terbium or cerium to the antisite defect define three possible variants of the crystalline field distortions, leading to the changes in the zero-field splitting Δ of Tb^{3+} ions and *g* factor values of Ce^{3+} ions. Thus, the presence of an antisite defect near the impurity rare earth ion of terbium or cerium should results in formation of three types of paramagnetic centers with parameters differing from the parameters of the ions in the regular environment. This agrees with the number of experimentally found additional centers of Tb^{3+} and Ce^{3+}. About 6% of terbium ions are close to the antisite defect, since the EPR signal intensity of each of the three centers is about 2% of the main Tb^{3+} EPR line intensity. A similar ratio observed for the cerium centers. This result agrees with the estimate made for the YAG:Ce crystal in [13]. As mentioned above, the antisite defect Y_{Al} causing changes in the EPR spectral parameters can be found in one of every ten octahedral positions of Al^{3+} in the environment of the impurity ion Tb^{3+} or Ce^{3+}; thus, the concentration of antisite defects in the studied crystal is approximately 0.6%.

The displacement of ions and the distortion of the immediate oxygen environment leads to a change in the crystal field, and hence to a change in the spectroscopic parameters. In the case of the Ce^{3+} ion, which does not have a fine structure (S = 1/2), this change manifests itself as a change in the values of the g factors. In the case of the non-Kramers Tb^{3+} ion, zero-field splitting is much more sensitive to changes of the crystal field. Such distortions from a defect of the $Y^{3+} \rightarrow Al^{3+}$ type lead to a decrease in the g_x component by 0.14. In the case of the non-Kramers Tb^{3+} ion associated with a defect Y_{Al} type center, the zero-field splitting increases by 34 GHz, and decrease by 12.8 GHz for $Al^{3+} \rightarrow Y^{3+}$ type defects in the immediate vicinity of the paramagnetic center.

In [17], using wide-band EPR spectroscopy, non-Kramers Ho^{3+} ions in yttrium aluminum garnet, which replace Y^{3+} ions in the dodecahedral positions of the crystal lattice were detected. The

formation of a quasi-doublet, within which resonant transitions were observed, is associated with the splitting of the main multiplet of the $^5I_8$ holmium ion in a crystal field of D_2 symmetry in the dodecahedral Y^{3+} site. Eight lines of hyperfine structure are observed, definitely indicating that the signals belong to the holmium ion (^{165}Ho, nuclear spin I = 7/2, natural abundance of 100%). Figure 4 show the EPR spectrum of Ho^{3+} ion in $Y_3Al_5O_{12}$. The figure shows only four of the eight components of the hyperfine structure for simplicity marked by arrows at the top.

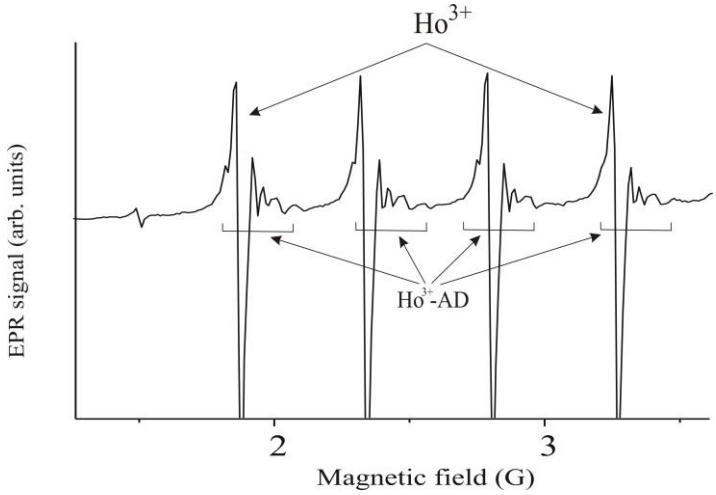

Fig. 4. EPR spectrum of Ho^{3+} ions in single crystals of yttrium aluminum garnet at T = 4.2 K, and ν = 170 GHz.

In addition to the main Ho^{3+} intensive lines in the spectrum, there are a number of satellite lines of lower intensity marked by arrows from below (Ho^{3+}-AD). They show the same hyperfine structure consisting of eight components as the main centers. The origin of these lines is associated with Ho^{3+} ions having an antisite defect in their environment. The sample orientation in magnetic field was chosen near **B** || [001] so that the resolution of the satellite lines was the best.

3. Conclusions

Thus, we can conclude that EPR spectroscopy, being sufficiently sensitive to changes in the nearest environment of a paramagnetic center can be used to detect and study transposition defects (antisite defects) both in yttrium-aluminum garnet crystals and in other materials.

Acknowledgments

The author is grateful to A.G. Petrosyan, N.G. Romanov, and G.S. Shakurov for interest in the work and help.

Funding

The research was carried out with the financial support of the Russian Foundation for Basic Research (RFBR Grant no. 20-52-05002 Arm_a).

References

[1] A. Kaminskii, Laser Crystals. Their Physics and Properties (Springer, Berlin, 1990).
[2] V. Bachmann, C. Ronda, A. Meijerink, Chem. Mater. **21** (2009) 2077.
[3] Y.S. Lin, R.S. Liu, B.-M. Cheng, J. Electrochem. Soc. **152** (2005) J41.

[4] A C. Dujardin, E. Auffray, E. Bourret-Courchesne, P. Dorenbos, P. Lecoq, M. Nikl, A. N. Vasil'ev, A. Yoshikawa, R. Zhu, IEEE Trans. Nucl. Sci. **65** (2018) 1977.
[5] P. Slyushev, K. Xia, R. Reuter, M. Jamali, N. Zhao, N. Yang, C. Duan, N. Kukharchyk, A. D. Wieck, R. Kolesov, J. Wrachtrup, Nat. Commun. **5** (2014) 3895.
[6] M.M. Kuklja, R. Pandey, J. Am. Ceram. Soc. **82** (1999) 2881.
[7] M.M. Kuklja, J. Phys.: Condens. Matter **12** (2000) 2953.
[8] Bo Liu, Mu Gu, Xiaolin Liu, Shiming Huang, Chen Ni, Appl. Phys. Lett. **94** (2009) 121910.
[9] A.B. Munoz-Garcia, E. Artacho, L. Seijo, Phys. Rev. B **80** (2009) 014105.
[10] A.B. Munoz-Garcia, Z. Barandiaran, L. Seijo, J. Mater. Chem. **22** (2012) 19888.
[11] M. Nikl, V.V. Laguta, A. Vedda, Phys. Status Solidi B **245** (2008) 1701.
[12] C.R. Stanek, K.J. McClellan, M.R. Levy, C. Milanese, and R.W. Grimes, Nucl. Instrum. Methods Phys. Res., Sect. A **579** (2007) 27.
[13] G.R. Asatryan, D.D. Kramushchenko, Yu.A. Uspenskaya, P.G. Baranov, A.G. Petrosyan, Phys. Solid State **56** (2014) 1150.
[14] E.V. Edinach, Y.A. Uspenskaa, A.S. Gurin, R.A. Babunts, H.R. Asatryan, N.G. Romanov, A.G. Badalyan, P.G. Baranov, Phys. Rev. B **100** (2019) 104435.
[15] Kh.S. Bagdasarov, Modern Crystallography (v. 3, Nauka, Moscow, 1980).
[16] A.G. Petrosyan, J. Cryst. Growth **139** (1994) 372.
[17] G.R. Asatryan, G.S. Shakurov, A.G. Petrosyan, D.D. Kramushchenko, K.L. Hovhannesyan, Phys. Solid State **64** (2022) 697.